Journal of Fluids and Structures (2001) **15,** 891–908
doi:10.1006/jfls.2001.0388, available online at http://www.idealibrary.com on IDEAL®

HYDRODYNAMIC DAMPING OF A LARGE SCALE SURFACE PIERCING CIRCULAR CYLINDER IN PLANAR OSCILLATORY MOTION

L. Johanning, P. W. Bearman and J. M. R. Graham

Department of Aeronautics, Imperial College of Science, Technology and Medicine London SW7 2BY, U.K.

(Received 20 December 2000, and in final form 10 March 2001)

Measurements of the hydrodynamic damping acting on a vertical, 0·5 m diameter cylinder in planar oscillatory motion at Stokes parameter, β, up to $1{\cdot}4 \times 10^5$ are presented. The results are also shown as a variation of drag coefficient, C_d, with Keulegan–Carpenter number, KC, where the range of KC numbers studied is from 1×10^{-3} to 1. The experiments were carried out in the Delta Flume at Delft Hydraulics Laboratories in Holland and the cylinder was mounted from a pendulum suspension system. The hydrodynamic damping is the sum of radiation damping, due to gravity waves generated by the cylinder piercing the water surface, and viscous damping. A frequency-domain solution from Dalrymple & Dean (1972) is used to predict the radiation damping. An estimate of the viscous damping is then obtained by subtracting the predicted radiation damping from the measured hydrodynamic damping. Results for the viscous damping derived in this way are found to be close to those expected from experimental studies carried out by Bearman & Russell (1996) and Chaplin & Subbiah (1996) to measure viscous damping on a submerged cylinder.

1. INTRODUCTION

In some modes of oscillation, compliant offshore structures such as TLPs have natural frequencies that are not far removed from the range of primary wave excitation. Typical natural frequencies in heave, pitch and roll correspond to periods of 2–4 s, while significant levels of the wave spectrum extend over a range of about 6–20 s. Nonlinearities in the waves and in wave/structure interaction at the so-called 'sum frequencies' raise possibilities of resonant excitation, and the consequences of second-order and third-order high frequency forcing have come to be known as springing and ringing.

Mechanisms for high frequency excitation, involving complex interactions in the vicinity of the water surface, have been studied analytically by a number of authors, assuming irrotational flow, and experimentally by Chaplin *et al.* (1997). Much less attention has been given to an equally important aspect of the problem of predicting responses and stresses, namely, the level of hydrodynamic damping. For a surface-piercing cylinder oscillating in still water, the hydrodynamic damping arises from two main sources: radiation damping due to the generation of waves and viscous damping. Viscous damping forces depend on the nature of the flow around oscillating bodies and in particular on the boundary layers, about which, at full scale, relatively little is known. The hydrodynamic damping of large compliant offshore structures acts mainly on cylindrical members having circular, rounded rectangular or rectangular cross-sections of dimensions of the order of 10 m. The resonant oscillations of concern have amplitudes as small as 1 cm, with frequencies around 0·3 Hz.

0889–9746/01/070891 + 18 $35.00/0

On the basis of these figures, order-of-magnitude estimates for the Reynolds number Re and Keulegan–Carpenter number KC for the oscillating flow are 2×10^5 and 0·006. However, in purely oscillatory flow, the Stokes parameter $\beta = \mathrm{Re}/\mathrm{KC} = D^2/\nu T$ is considered more appropriate than the Reynolds number as a measure of the importance of viscosity, and for the full-scale conditions described above, $\beta \sim 3 \times 10^7$.

Though in the past much experimental work has been devoted to the loading on fully submerged cylinders in oscillatory flow, the regime of very small KC numbers, appropriate to the case of TLP damping in still water, has received much less attention and examples include the work of Bearman & Russell (1996) and Chaplin & Subbiah (1996). Earlier measurements at higher values of KC, but still less than 1, are described by Sarpkaya (1986a) and Otter (1990). For practical reasons, all these measurements were carried out at values of β of more than two orders of magnitude lower than those appropriate to full-scale conditions.

The flow around an oscillating circular cylinder with an attached, two-dimensional, laminar boundary layer was first treated by Stokes (1851). He developed a solution for the damping force, which was later extended by Wang (1968) by using the method of inner and outer expansions. Using Wang's result, the parts of the force in-phase and out of phase with the motion can be related to the drag coefficient, C_d, and inertia coefficient, C_m, used in Morison's equation to give

$$C_d = \frac{3\pi^3}{2\mathrm{KC}} [(\pi\beta)^{-1/2} + (\pi\beta)^{-1} - \tfrac{1}{4}(\pi\beta)^{-3/2}], \tag{1}$$

$$C_m = 2 + 4(\pi\beta)^{-1/2} + \tfrac{1}{4}(\pi\beta)^{-3/2}. \tag{2}$$

These expressions are only valid for $\mathrm{KC} \ll 1$, $\mathrm{ReKC} \gg 1$ and $\beta \gg 1$. For high β values, the drag coefficient reduces to just the first term in equation (1),

$$C_d = \frac{3\pi^3}{2\mathrm{KC}} (\pi\beta)^{-1/2} = \frac{26{\cdot}24}{\mathrm{KC}\sqrt{\beta}}. \tag{3}$$

Though it cannot be expected to be valid in conditions where the boundary layer is turbulent, or where the flow is in some other way three dimensional, Wang's result provides a useful reference point for C_d and is hereafter referred to as W. The measurements of Sarpkaya (1986a) and Otter (1990) confirmed that at KC numbers below a certain threshold (depending on the value of β), the drag coefficient becomes inversely proportional to KC, in agreement with equation (3); but otherwise Sarpkaya's and Otter's results, at around, respectively, $\beta = 1{\cdot}1 \times 10^4$ and $\beta = 6{\cdot}2 \times 10^4$, differ markedly from each other. From measurements down to $\mathrm{KC} = 0{\cdot}8$ Sarpkaya found $C_d \approx 5\mathrm{W}$, while for $\mathrm{KC} > 0{\cdot}03$ Otter reported $C_d \approx \mathrm{W}$. However, it seems unlikely that measurements of drag coefficient at β values as high as $6{\cdot}2 \times 10^4$ should agree with the two-dimensional laminar flow result.

The measurement of drag on a body in a relative oscillating flow of small amplitude brings about experimental problems that are not encountered in the so-called Morison regime, where the drag and inertia components of the force are of roughly similar magnitudes. When a cylinder is driven through fluid initially at rest with a prescribed harmonic motion of small amplitude at high β, the ratio of the amplitudes of the drag and inertia forces (assuming that $C_d = 1$ and $C_m = 2$) is $1{\cdot}3/\sqrt{\beta}$. This ratio is 0·01 at $\beta = 1{\cdot}7 \times 10^4$, causing severe difficulties in the calculation of reliable estimates of drag coefficients (and therefore of hydrodynamic damping) from measurements of forces or pressures on the cylinder.

Bearman & Russell (1996) avoided this problem by measuring the decaying oscillations of submerged cylinders mounted beneath a pendulum. The drag coefficient is directly related to the logarithmic decrement of the motion, and so a single test run provided results over a range of KC numbers at constant β. Facing the same problem, Chaplin & Subbiah (1996) developed a test rig in which the cylinder was elastically mounted under water and excited at resonance by an externally applied oscillating force of constant amplitude. In this case, measurement of the amplitude and phase of the cylinder response in each test provided the drag coefficient for a particular KC and β. In both sets of experiments, it was necessary to take particular care over accounting for the fluid loading on supporting struts and end plates. For small KC, the drag coefficient in both sets of experiments was found to be inversely proportional to KC. At $\beta \approx 7 \times 10^4$, Bearman & Russell found $C_d \approx 2\text{W}$, and at $\beta \approx 1{\cdot}7 \times 10^5$. Chaplin & Subbiah found $C_d \approx 2{\cdot}2\text{W}$.

From an analysis of their drag coefficient measurements for a smooth cylinder, Bearman & Russell (1996) proposed the following relationship for the variation of C_d with KC at high values of β:

$$C_d = \frac{2 \times 26{\cdot}24}{KC\sqrt{\beta}} + 0{\cdot}08\text{KC}. \tag{4}$$

This expression is valid for KC values up to about 5 but at the low KCs studied in this paper the second term can be neglected. Hence equation 4 reduces to $C_d = 2\text{W}$.

It is not known how the drag coefficient will change with further increases in β, and, possibly more important, it is not known what structural changes will take place in the boundary layer with further increases in scale. As flow visualisations by Honji (1981), and later by Bearman & Mackwood (1992), have shown, the boundary layer on an oscillating cylinder, depending on the values of KC and β, has an organised three-dimensional structure that must influence the loading on it. At some higher value of the Stokes parameter, this structure is likely to break down and be replaced by a fully developed turbulent flow characterised possibly by a β-independent drag coefficient. Large scale experimental work by Bearman *et al.* (1985) helped to identify the onset of such post-critical conditions in wave flow around a cylinder in the Morison regime at higher KC numbers, but these conclusions are unlikely to apply in the present case.

In addition to the influence of β on the drag of a cylinder, it is known that the roughness of the surface also has an effect. Sarpkaya (1986a) tested a rough cylinder at $\beta = 1800$ with a relative roughness $k/D = 1/100$ (where k is the surface roughness and D the cylinder diameter) for a range of KC-numbers ($\text{KC} > 0{\cdot}4$) and found an increase in C_d compared to a smooth cylinder. In later investigations, Sarpkaya found $C_d \approx 3.2\text{W}$ for a rough cylinder with a relative roughness $k/D = 1/100$ and $C_d \approx 2{\cdot}2\text{W}$ for a smooth cylinder at a β-value around 1×10^6 (Sarpkaya 2000). Bearman & Mackwood (1992) tested three different roughnesses ($k/D = 1/50$, $k/D = 1/100$ and $k/D = 1/200$) for β-values from $1{\cdot}4 \times 10^4$ to $2{\cdot}1 \times 10^4$ and compared the results with the results obtained for a smooth cylinder. They found an increase in C_d above the smooth cylinder values for the relative roughnesses of $k/D = 1/50$ and $k/D = 1/100$. For the surface finish with $k/D = 1/200$ they found results close to those obtained with a smooth cylinder. This disagrees with a result from Chaplin and Subbiah (1998) who tested a rough cylinder with a much lower relative roughness of $k/D = 1/1300$, in the low Keulegan–Carpenter regime, for a Stokes parameter β of $1{\cdot}7 \times 10^5$ and they found $C_d = 3\text{W}$.

In this paper we present results from experiments carried out in the Delta Flume at Delft Hydraulics Laboratories to measure hydrodynamic damping at large scale. Measurements were made on a 0·5 m diameter, vertical, circular cylinder that pierced the water surface. The

investigation included measurements made on the cylinder oscillating in still water, oscillating in-line and transverse to waves, oscillating in-line and transverse to a current and oscillating in a combined wave and current flow. Here, we limit the presentation of results to those for planar oscillatory flow. Since the cylinder passed through the water surface it radiated waves to the surrounding fluid, and this generated an additional radiation damping force. To be able to estimate the drag coefficient due to viscous forces, it is necessary to subtract the radiation damping from the total damping in order to obtain the viscous damping. A frequency-domain solution due to Dean & Dalrymple (1972) is used to find the radiation damping. It will be shown that, depending on the flow parameters, the radiation damping can have a large influence on the total damping.

2. EXPERIMENTAL ARRANGEMENT

The experiments were carried out in the Delta Flume at Delft Hydraulics in Holland. This tank is 230 m long and 5 m wide and for the present experiments it was filled to a mean water depth of 5 m. The tank is equipped with a piston-type wave paddle that can generate waves with heights up to 2 m. There is a carriage that runs along the tank on rails with a maximum speed of 1 m/s and this can be used to simulate the effect of a current. For the still water experiments described here, the magnetic brakes on the carriage were applied and in addition the wheels were blocked. The total weight of the carriage, with additional mass added, was 30 000 kg and this provided a stable base on which the cylinder suspension system was to be mounted. The experiments were conducted outdoors but during the measurement programme the winds were very light and it was not thought that atmospheric conditions had any influence on the results.

For the experiments, a 7·1 m long and 500 mm diameter hollow steel circular cylinder with a wall thickness of 10 mm and a total mass $m_{\text{cyl}} = \sim 1200$ kg was constructed by welding together three sections. The cylinder passed through the water surface and its immersed length was 4·78 m (Figure 1), which for small amplitudes of oscillation gives an added mass, m_a, of 940 kg. Throughout the experimental programme there was no sign of any water leaking into the cylinder. In order to simulate a surface typically found on sections of offshore structures, the cylinder with diameter D was covered with a waterproof abrasive sheet, which gave a relative roughness of $k/D \simeq 1/8000$. (It should be noted that in a few places some small ripples appeared in the abrasive sheet, locally increasing k/D to $\sim 1/150$.)

The apparatus used to suspend the cylinder was a larger version of the double pendulum system employed by Bearman & Russell (1996). The support system was constructed using a double 'A-frame' (Figure 1) with a height of 4 m, and a base 3 m × 2·5 m that was firmly attached to the carriage. This system had a total weight of ~ 4 tonnes, which was in addition to the weight of the carriage mentioned earlier. The frame was constructed from 150 mm hollow square steel sections and four pendulum arms, made from 120 mm hollow square steel sections, were used in the form of a 'double pendulum' system. The pendulum arms were attached to the support system and the pendulum base using flexures manufactured from spring steel with dimensions 50 × 30 × 3 mm. The pendulum base provided the attachment for the cylinder, a release mechanism, a means for changing the frequency of oscillation and attachments to allow calibrations to be carried out. The effective earth point for the release mechanism and the frequency adjustment and calibration arrangements was an adjustable table, manufactured from 120 mm hollow square steel sections, that was fastened solidly to the lower end of the pendulum support system. The clearance between the pendulum base and the adjustable table provided for a normal cylinder displacement of 100 mm with an adjustment of ± 50 mm. The cylinder moved in predominately horizontal

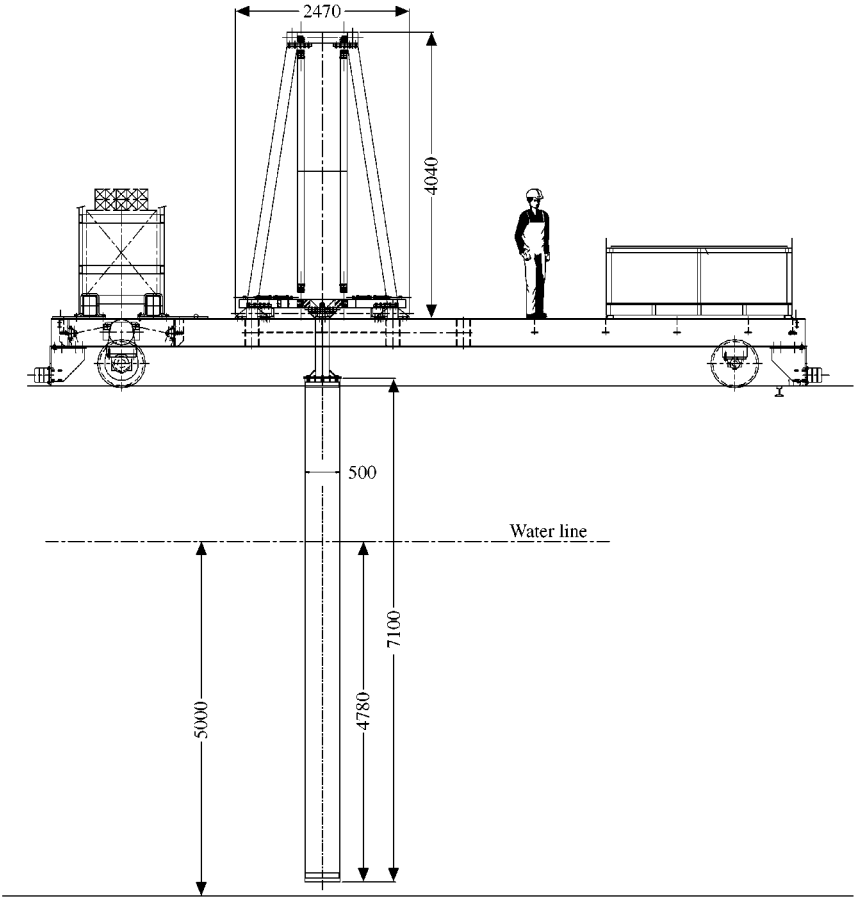

Figure 1. Scaled design drawing of experimental set-up; Dimensions are in mm.

motion combined with a very small vertical displacement. Bearman & Russell (1996) found that this small motion along the direction of the cylinder axis did not affect measurements of hydrodynamic damping.

A worm gear winch with a capacity of 1000 kg was used to displace the pendulum from its neutral position. Four 24V DC Magnets with a total capacity of 1200 kg were then used to hold the pendulum and cylinder at an initial displacement (Figure 2). To release the cylinder, the magnets were either switched off by using a trigger impulse or by hand. In order to adjust the frequency of the system, a series of springs were used (Figure 2), connected between the lower end of the pendulum and the base. This provided a possible frequency range from 0·167 to 0·941 Hz, giving β values from $4{\cdot}16 \times 10^4$ up to $2{\cdot}34 \times 10^5$.

In order to find the effective mass per unit length M of the system, the following relationship was used:

$$M = \frac{\kappa_h}{(2\pi f_h)^2 L}, \tag{5}$$

where κ_h = stiffness, f_h = frequency in water and L = immersed cylinder length. To obtain the stiffness in water, a calibrated weight was suspended over a pulley (Figure 2). By

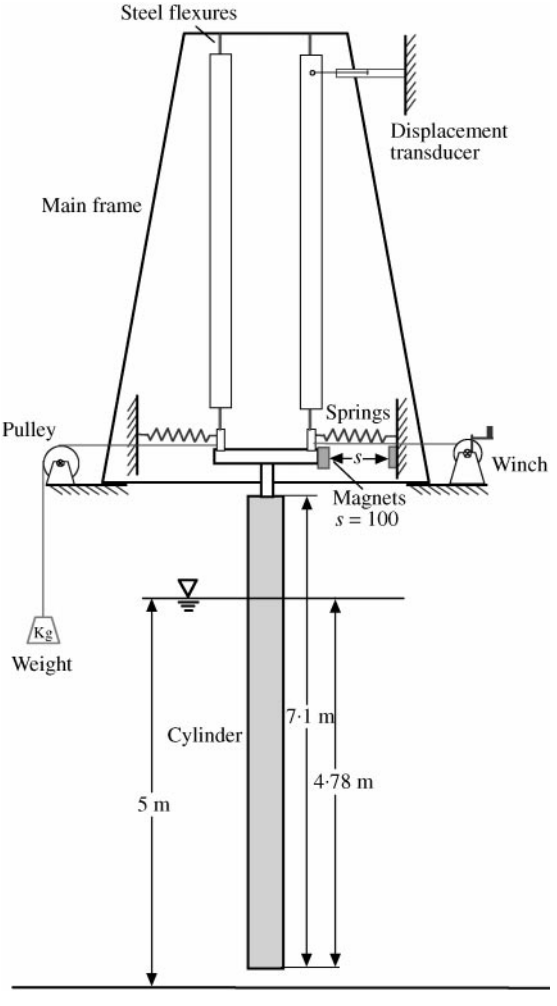

Figure 2. Experimental arrangement.

measuring the resulting displacement the stiffness of the system can be determined, and then by measuring the oscillation frequency the effective mass can be determined. In order to obtain the oscillating displacement, a miniature DC energised LVD transducer with very small friction and a maximum stroke of 15 mm was attached near the top of the pendulum arms, between the arms and the pendulum support system (Figure 2). The transducer was carefully calibrated and the output was used to calculate the KC number, as well as providing time histories of the decaying motion. Calibrations were carried out before and after a series of experiments and the maximum differences recorded were $\sim \pm 1\%$. The effective masses per unit length for the four frequencies tested are given in Table 1, together with stiffnesses and the frequencies measured in air and water.

3. EXPERIMENTAL METHOD AND THEORETICAL BACKGROUND

The hydrodynamic damping of a body is directly linked to the drag acting on it and in this paper, measurements of damping will be used to calculate drag coefficients. In the present experiments it is assumed that the hydrodynamic force on the cylinder in oscillatory motion

TABLE 1
Experimental conditions

Experiment	f_a	f_h	Stokes parameter β-value	ζ_a	ζ_h	κ_h	$\frac{M}{\rho D^2}$	Reduced damping		
								Hydrodynamic	Radiation	Viscous
								ζ_{r_h}	ζ_{r_w}	ζ_{r_v}
SP00	0·283	0·167	$4{\cdot}16 \times 10^4$	0·0014	0·0050	$2{\cdot}98 \times 10^3$	2·23	0·142	0·0063	0·1357
SP02	0·492	0·366	$9{\cdot}13 \times 10^4$	0·0011	0·0075	$1{\cdot}52 \times 10^4$	2·39	0·226	0·101	0·125
SP04	0·625	0·470	$1{\cdot}17 \times 10^5$	0·0012	0·0090	$2{\cdot}73 \times 10^4$	2·55	0·290	0·179	0·111
SP06	0·725	0·548	$1{\cdot}37 \times 10^5$	0·0013	0·0097	$3{\cdot}95 \times 10^4$	2·75	0·334	0·240	0·094

can be represented by Morison's equation. This well known equation expresses the total force per unit length as the sum of drag and inertia force components and is given by

$$F = \frac{1}{2}\rho D C_d \dot{x}|\dot{x}| + \frac{\pi D^2}{4}\rho C_m \ddot{x}, \tag{6}$$

where $\dot{x}$ is the velocity and $\ddot{x}$ the acceleration of the body and ρ is water density. However, it should be noted that in the experiments described here the total damping is the sum of hydrodynamic damping and structural damping and the hydrodynamic damping is composed of viscous damping and wave radiation damping components. Hence, by measuring the decay of $\hat{x}_i$, the peak amplitude of the cylinder during a cycle, over N cycles the total damping is given by

$$2\pi N(\zeta_0 + \zeta_w + \zeta_v) = \log\left(\frac{\hat{x}_i}{\hat{x}_{i+N}}\right), \tag{7}$$

where ζ_0 is the structural damping, ζ_w is the radiation damping and ζ_v is the viscous damping. The hydrodynamic damping, ζ_h is

$$\zeta_h = \zeta_v + \zeta_w. \tag{8}$$

Figure 3(b) shows a typical time history of a decaying oscillation in water. The damping, found from decaying oscillations, is often expressed in the form of a reduced damping coefficient given by

$$\zeta_r = \frac{2M(2\pi\zeta_v)}{\rho D^2}. \tag{9}$$

Similar expressions can be defined for the other components of damping and the total damping.

3.1. STRUCTURAL DAMPING

The structural damping was found experimentally by measuring the decaying motion of the cylinder in air for a variety of frequencies. Over N cycles of motion, the structural damping is given by

$$2\pi\zeta_0 = \left\{\frac{\log(\hat{x}_i/\hat{x}_{i+N})}{N}\right\}_{\text{air}}. \tag{10}$$

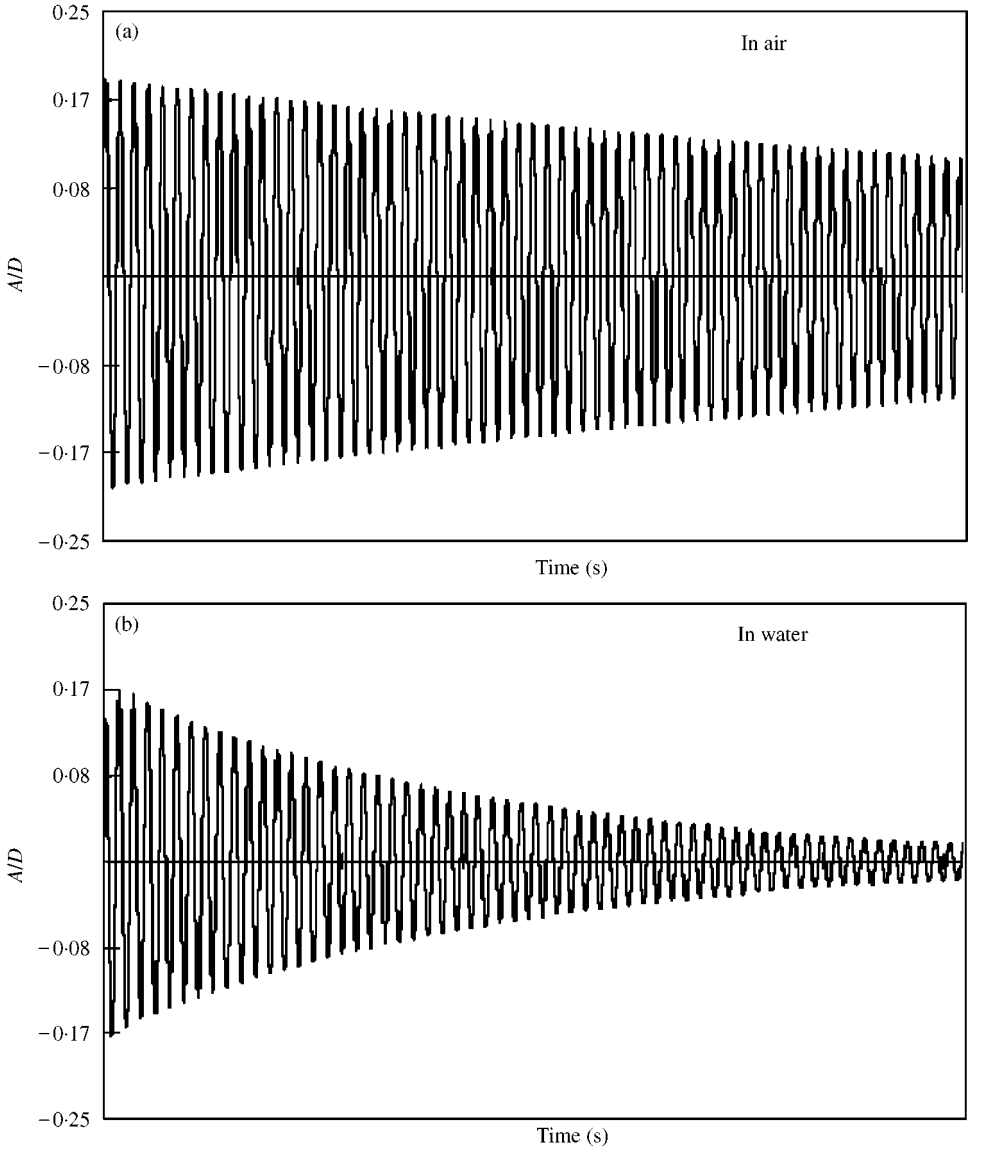

Figure 3. Decaying oscillation in air and water.

The decay tests were carried out three times for each frequency, with similar results for all three runs, and the mean damping was found. Figure 3(a) shows a typical time history of the decaying oscillation in air and Figure 4 shows the damping factor ζ_0 versus the dimensionless amplitude, A/D. The structural damping factor is given in Table 1 for the four frequencies tested.

3.2. Radiation Damping

Oscillating structures radiate waves to a surrounding fluid and the force on the body due to the generation of these waves, F_w, is the sum of a component in phase with the

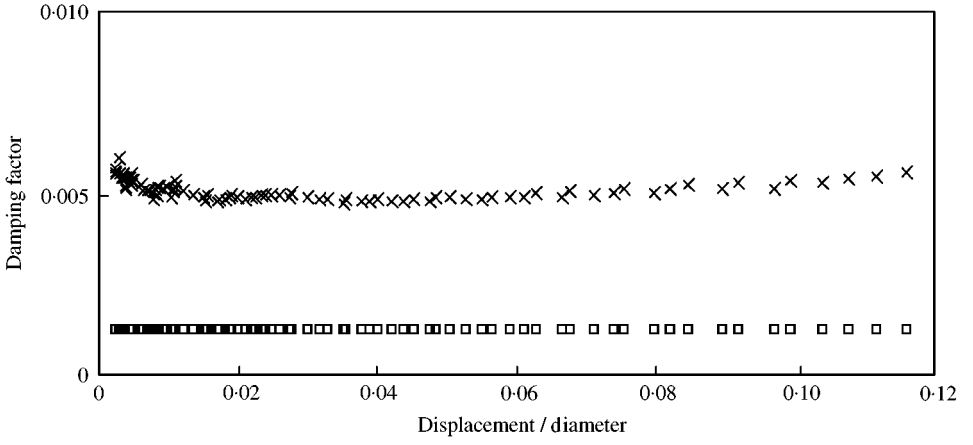

Figure 4. Damping factor versus dimensionless amplitude in air and water ($f_h = 0{\cdot}167$, $\beta = 4{\cdot}16 \times 10^4$, $\zeta_0 = 0{\cdot}0014$, $\zeta_h = 0{\cdot}005$, $\zeta_{r_h} = 0{\cdot}142$): ×, hydrodynamic damping; □, structural damping.

body's velocity and a component in phase with its acceleration (Sarpkaya & Isaacson 1981),

$$F_{w_i} = -\sum_{j=1}^{6} (\mu_{ij}\ddot{x}_j + \lambda_{ij}\dot{x}_j) \qquad \text{for } i = 1, 2, \ldots, 6, \tag{11}$$

where $\dot{x}_j$ is the velocity and $\ddot{x}_j$ is the acceleration of the body. The subscript j relates to the six components of motion of a floating body, i.e., for translational motion; surge, sway and heave and for the rotational motion: roll, pitch and yaw. The terms μ_{ij} and λ_{ij} are the added mass and damping due to wave radiation. The equation of motion for an oscillating body can be written in the form

$$F_{w_j}^{(e)} = (m_{ij} + \mu_{ij})\,\ddot{x}_j + \lambda_{ij}\dot{x}_j + \kappa_{ij}x_{ij}, \tag{12}$$

where m_{ij} is the mass of the system and κ_{ij} is the system stiffness. It should be noted that equation (12) does not include any structural or viscous damping terms and relates solely to wave radiation. The added mass and damping can be expressed as

$$\mu_{ij} = \frac{\mathrm{i}\rho}{\omega^2} \int_{S_0} \mathrm{Im}[\phi_j^{(f)}]\, \frac{\partial \phi_i^{(f)}}{\partial n}\, \mathrm{d}S, \tag{13a}$$

$$\lambda_{ij} = \frac{\mathrm{i}\rho}{\omega} \int_{S_0} \mathrm{Re}[\phi_j^{(f)}]\, \frac{\partial \phi_i^{(f)}}{\partial n}\, \mathrm{d}S, \tag{13b}$$

where Re[ ] and Im[ ] represent real and imaginary parts, ω is frequency, ρ is fluid density, S is volume of the body per unit length and $\phi_j^{(f)}$ is the velocity potential due to the body motion. The energy input into the body required to produce wave radiation is given by

$$E = -\sum\nolimits_i \hat{F}_{w_e}\hat{\dot{x}}_i = \sum_{i,j} \lambda_{ij}\hat{\dot{x}}_i\hat{\dot{x}}_j, \tag{14}$$

where only the damping coefficient is associated with the dissipated energy and the part from the added mass vanishes due to the periodicity of the flow (Mei 1983).

There are relatively few analytic solutions for predicting wave radiation from oscillating bodies but the case of a vertical, surface piercing circular cylinder has been treated by

a number of authors. A frequency-domain solution due to Dalrymple & Dean (1972) [see also Dean & Dalrymple (1993)] is used here to calculate the hydrodynamic damping due to wave radiation for a cylinder in planar oscillatory motion. The lower end of the cylinder is presumed to slide over the bed with zero friction and the flow is assumed to be inviscid such that a velocity potential, which is a solution of Laplace's equation, can be defined. A linearized boundary condition is applied at the free surface of the water. Clearly, there are viscous effects present in the real flow but at the very small KC numbers treated here they will be confined to a thin boundary layer around the cylinder and are expected to have a negligible influence on the wave radiation-damping component. Complete details of the method of the solution can be found in the references cited above and only the results will be presented here.

Using results from Dean & Dalrymple (1972), the energy input from the cylinder to produce a wave is given by

$$E = \frac{|A_o|^2(\sinh 2kh + 2kh)}{2k}\, 2\pi\rho, \tag{15}$$

where h is the water depth and k is the wave number. For a sway motion of the cylinder, which has constant amplitude with depth, the coefficient A_o becomes

$$A_o = \frac{2\omega a\hat{x}_{11}\sinh(k_0h)\,\mathrm{e}^{-\mathrm{i}v}}{\sinh(2k_0h) + 2k_0h}\,\frac{1}{(ak_0)[\mathrm{H}_1^{(1)}(k_0a)]'}, \tag{16}$$

where $v = \tan^{-1}(\mathrm{Y}_1'(k_0a)/\mathrm{J}_1'(k_0a))$ is the phase angle and $\mathrm{H}_1^{(1)}(k_0a)$ is the Hankel function of the first kind, where $\mathrm{Y}_1(k_0a)$ and $\mathrm{J}_1(k_0a)$ are Bessel functions.

The equation of motion for the cylinder is assumed to be that for an ideal mass–spring–damper system,

$$m\ddot{x}_{11} + b\dot{x}_{11} + \kappa x_{11} = 0. \tag{17}$$

The dissipated energy by damping over one cycle is given by

$$\Delta E_w = \int_t^{t+T} \hat{F}\,\frac{\mathrm{d}\hat{x}_{11}}{\mathrm{d}t}\,\mathrm{d}t \equiv \int_t^{t+T} \hat{F}\dot{\hat{x}}_{11}\,\mathrm{d}t. \tag{18}$$

If the oscillation is harmonic, then the energy over one cycle is

$$\Delta E_w = ML\omega^2\hat{x}_{11}^2(2\pi\zeta_w). \tag{19}$$

If we equate the dissipated energy over one cycle to the energy required to radiate waves during one cycle, we can obtain an expression for the damping factor due to wave radiation,

$$\zeta_w = \frac{4\rho a^3(\sinh(k_0h))^2}{ML(\sinh(2k_0h) + 2k_0h)}\,\frac{(\mathrm{e}^{-\mathrm{i}v})^2(\mathrm{H}(k_0a))^2}{k_0a}, \tag{20}$$

where $\mathrm{H}(k_0a) = \{(k_0a)[\mathrm{H}_1^{(1)}(k_0a)]\}^{-1}$.

In Figure 5 the radiation damping given by equation (20) is plotted against ka for a ratio of cylinder radius to water depth appropriate to the experiments of $a/h = 0{\cdot}05$. Assuming that deep water waves are generated by the small amplitude motion of the cylinder then, from the dispersion relationship, $ka = \omega^2 a/g$. It can be seen that the damping increases rapidly with ka, reaching a maximum at about $ka = 0{\cdot}7$, and then continuously falls with further increases in ka. The symbols shown in the figure are the theoretical values of radiation damping appropriate to the four test cases given in Table 1 and it can be seen that they all lie on the steeply rising portion of the curve.

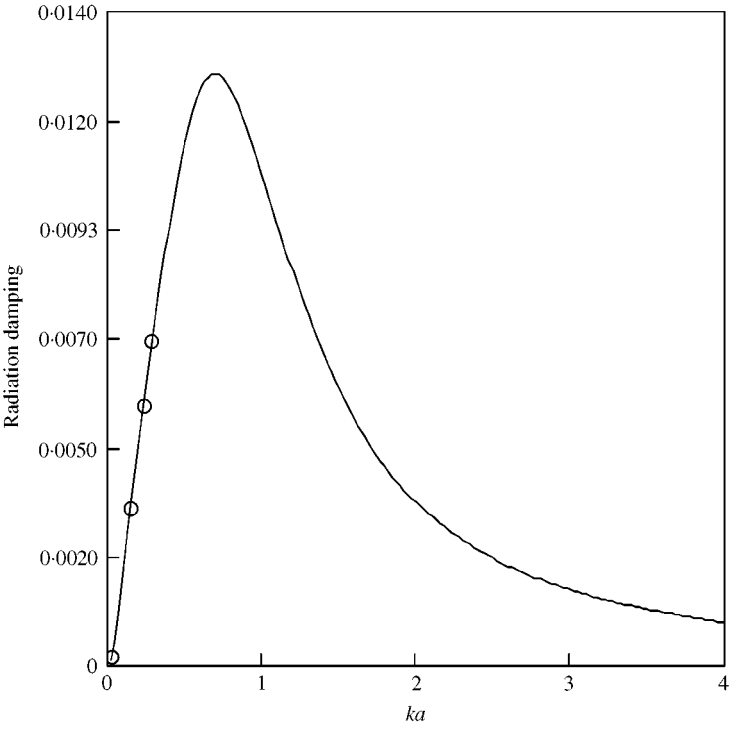

Figure 5. Estimated radiation damping for a range of gravity wave parameter for $a/h = 0{\cdot}05$: —, theoretical solution Dalrymple & Dean; ○○○, theoretical damping for experiments.

3.3. Viscous Damping

A structure vibrating in a viscous fluid experiences hydrodynamic damping due to viscous drag forces. The hydrodynamic force acting on an oscillating cylinder is assumed to be given by Morison's equation [equation (6)] and the equation of motion for the cylinder becomes

$$M\ddot{x} + 2M\zeta_s\omega\dot{x} + \kappa_h x = F_D = -\tfrac{1}{2}\,\rho D C_d\,|\dot{x}|\,\dot{x}. \tag{21}$$

Here, M is the total mass per unit length, including the added mass component from Morison's equation, ζ_s the structural damping, ω the structural natural frequency, κ_h the stiffness of the structure, ρ density of fluid, D the cylinder diameter, C_d the drag coefficient and x the structure displacement. It should be noted that equation (21) includes the structural damping but not the radiation damping.

As the structure undergoes harmonic motion with amplitude $\hat{x}$, the structure velocity can be expressed as

$$\dot{x}(t) = \omega\hat{x}\cos(\omega t). \tag{22}$$

Then, by expanding the nonlinear term on the right-hand side of equation (21) as a Fourier series and taking just the leading term, this becomes

$$\begin{aligned} |\dot{x}|\dot{x} &= \hat{x}^2\,\omega^2|\cos(\omega t)|\cos(\omega t) \\ &\approx \frac{8}{3\pi}\,\hat{x}^2\omega^2\cos(\omega t) = \frac{8}{3\pi}\,\hat{x}\omega\dot{x}. \end{aligned} \tag{23}$$

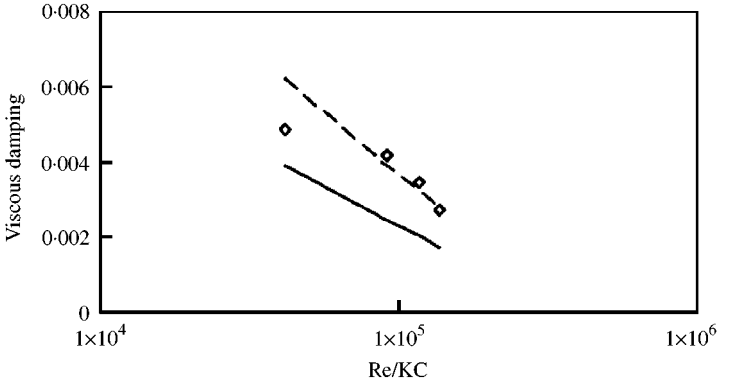

Figure 6. Estimated and experimental viscous damping for different β-values: ◇◇◇, experimental; —, theoretical (2W); – –, theoretical (3·2W).

The equation of motion can then be rewritten as

$$M\ddot{x} + 2M\omega\left[\zeta_s + \frac{4}{3\pi}\frac{\rho D^2}{2M(2\pi)}C_d\,\mathrm{KC}\right]\dot{x} + \kappa_h x = 0 \tag{24}$$

and the viscous damping is

$$\zeta_v = \frac{4}{3\pi}\frac{\rho D^2}{2M(2\pi)}C_d\,\mathrm{KC}, \tag{25}$$

where the drag coefficient is unknown. By adopting equation (4) for the drag coefficient and by noting that the right hand term becomes insignificant for $\mathrm{KC} \ll 1$, an estimate of the viscous dampings can be calculated from

$$\zeta_v = \frac{1}{3\pi^2}\frac{\rho D^2}{M}\frac{2\times 26{\cdot}24}{\sqrt{\beta}}. \tag{26}$$

The hydrodynamic damping is the sum of the viscous and radiation damping [equation (8)] and hence the viscous damping can be found by subtracting the radiation damping given by equation (20) from the experimental found hydrodynamic damping ζ_h. In Figure 6, estimated viscous damping values are compared with the damping found from the experimental study. The estimated viscous damping is calculated from equation (26) for a smooth cylinder by using the relationship $C_d = 2\mathrm{W}$ (Bearman & Russell 1996) and from equations (25) and (4) by applying $C_d = 3{\cdot}2\mathrm{W}$ (Sarpkaya 2000) for a rough cylinder.

To be able to calculate the drag coefficient from the experimental viscous damping, equation (25) is rearranged and the relationship in equation (8) is used to express the viscous damping

$$C_d = \frac{3\pi}{4\mathrm{KC}}\frac{2M[2\pi(\zeta_h - \zeta_w)]}{\rho D^2} = \frac{3\pi}{4}\frac{\zeta_r}{\mathrm{KC}}. \tag{27}$$

4. EXPERIMENTAL RESULTS AND DISCUSSION

Measurements of hydrodynamic and structural damping factors are shown plotted in Figure 4 against cylinder amplitude, for a cylinder frequency in water of 0·167 Hz (case SP00). It can be seen that there is very little variation of damping with cylinder

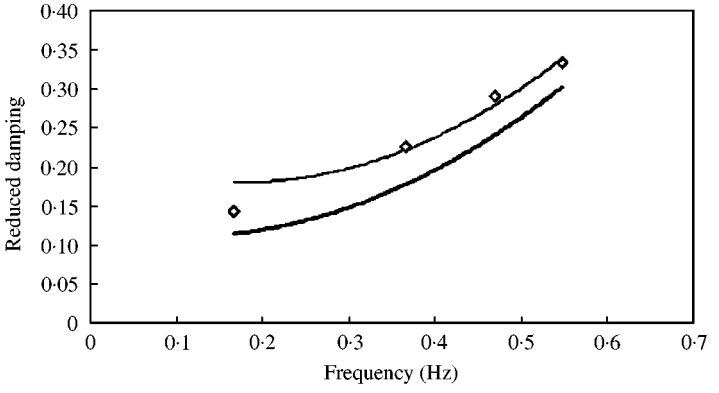

Figure 7. Theoretical and experimental hydrodynamic damping for different frequencies: ◇, hydrodynamic damping (experimental); —, hydrodynamic damping (theoretical {2W}); —, hydrodynamic damping (theoretical {3·2W}).

displacement. Damping factors for all four frequencies tested are given in Table 1. Further, the measured hydrodynamic damping, expressed as a reduced damping, is plotted in Figure 7 against cylinder frequency measured in water. The hydrodynamic damping is observed to increase steadily with increasing frequency. Since the hydrodynamic damping is generated by two completely different physical processes, there is no natural way to present the damping as a function of a nondimensional frequency. If the predominant component is viscous damping then it could be presented as a function of β, whereas if it is radiation damping then the appropriate nondimensional frequency would be $\omega^2 a/g$.

Also shown in Figure 7 are estimates of hydrodynamic damping obtained by combining radiation damping from equation (20) and viscous damping from equation (25) and equation (4) by applying $C_d = 2\text{W}$ for a smooth cylinder and $C_d = 3{\cdot}2\text{W}$ for a rough cylinder. It is interesting to note that the estimate for the hydrodynamic damping using the relationship $C_d = 3{\cdot}2\text{W}$ shows a close agreement with the experimental results. Roughness (k/D) influences only the viscous damping and an increase above smooth cylinder values has been shown for a k/D-number down to 1/100 by Sarpkaya (1986a, 2000) and Bearman & Mackwood (1992) and down to 1/1300 by Chaplin & Subbiah (1998). There is an uncertainty as to how much the damping is influenced at even smaller k/D-values and it is not known at what level of k/D a cylinder surface can be called smooth. Bearman & Mackwood (1992) found a very small increase in damping for $k/D = 1/200$, whereby Chaplin & Subbiah found $C_d = 3\text{W}$ for a relative roughness $k/D = 1/1300$. The relative roughness tested in this study of $k/D = 1/8000$ is some times smaller than that tested by Chaplin & Subbiah, and corresponds to a roughness height of 1·5% of the nominal thickness of the Stokes layer in laminar oscillatory flow ($5D(\pi\beta)^{-1/2}$). While an increase in drag is not expected for this small relative roughness, it should be noted that a small amount of rippling appeared on the abrasive sheet which increased k/D locally to 1/150.

It can easily be shown that the growth in hydrodynamic damping with frequency illustrated in Figure 7 is due to an increase in radiation damping. The radiation damping derived from equation (20) is plotted in Figure 8 for the four frequencies that are tested. Plotted in the same figure is the viscous damping obtained from the empirical expression given in equation (26). Whereas viscous damping is predicted to fall with increasing frequency, radiation damping increases. By increasing the oscillation frequency the value of β increases and, as shown by equation (26), viscous damping is expected to fall. The viscous damping found by subtracting the radiation damping from the measured total

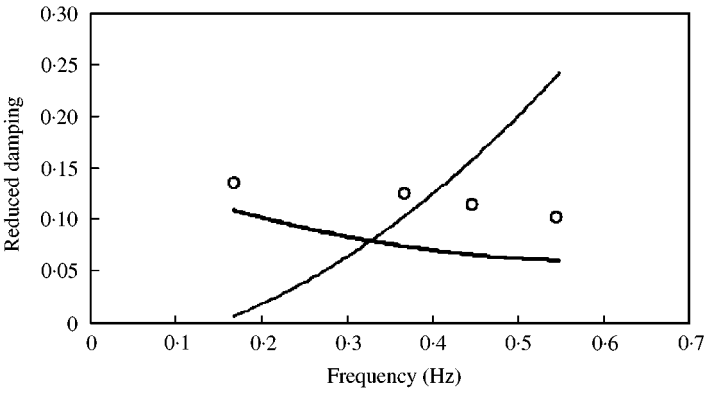

Figure 8. Comparison of analytical and experimental viscous damping and estimated radiation damping: ○, viscous damping (experimental); —, viscous damping (theoretical {2W}); —, radiation damping.

hydrodynamic damping, is also shown as plotted in Figure 8. The viscous damping derived in this way follows a similar trend with frequency to that predicted by equation (26) but the level is higher, which indicates a C_d value greater than 2W. Reduced damping values for radiation and viscous effects are given in Table 1.

While it should be noted that there is likely to be some uncertainty in the estimates of both radiation and viscous damping, the method of presentation used in Figure 8 apparently places all the error on viscous damping. It can be seen from Figure 5 that in the range of the experimental parameters the radiation damping rises sharply with increasing *ka*, so a small error in calculating the frequency of oscillation will lead to a large error in damping. The viscous damping plotted in Figure 8 is being compared with values obtained from experiments where the end conditions on the cylinder are quite different. In the experiments of Bearman & Russell (1996), end-plates were fitted to the cylinder whereas in the present work, there are no end-plates. This will have some influence on the estimates of viscous damping.

The measurements of damping are undoubtedly influenced by extraneous structural effects, which need some further explanation. Although the carriage wheels were locked, some vibration of the carriage structure could be detected and this became more pronounced for experiments carried out at higher cylinder frequencies. Also, the vibrations became more noticeable when the cylinder was immersed in water. Hence, it is expected that the structural damping, measured in air, is smaller than the actual structural damping when the cylinder is in water. This increase of the structural damping in water cannot be quantified but it will lead to an overestimate of the hydrodynamic damping, especially for experiments at high β values. A second unwanted vibration was observed when the springs were in place to increase the frequency of the cylinder. A first-mode bending of the cylinder was excited which introduced a frequency of 2 Hz into the system. This limited the highest frequency that could be tested and the experiments had to be restricted to a frequency of 0·548 Hz that gave a maximum β-value of $1{\cdot}37 \times 10^5$.

Drag coefficients, estimated according to equation (27), are plotted against Keulegan–Carpenter number, for four different β values, in Figure 9(a–d). Also shown is the theoretical prediction by Wang (1968) for laminar flow and the empirical prediction of Bearman & Russell (1996). In all cases, at low KC the drag coefficients estimated from the present experiments are larger than the values predicted by Bearman & Russell. This is reflected in the higher values of viscous damping seen in Figure 8. The most likely sources of additional viscous damping are related to the omission of an end plate on the bottom of the cylinder

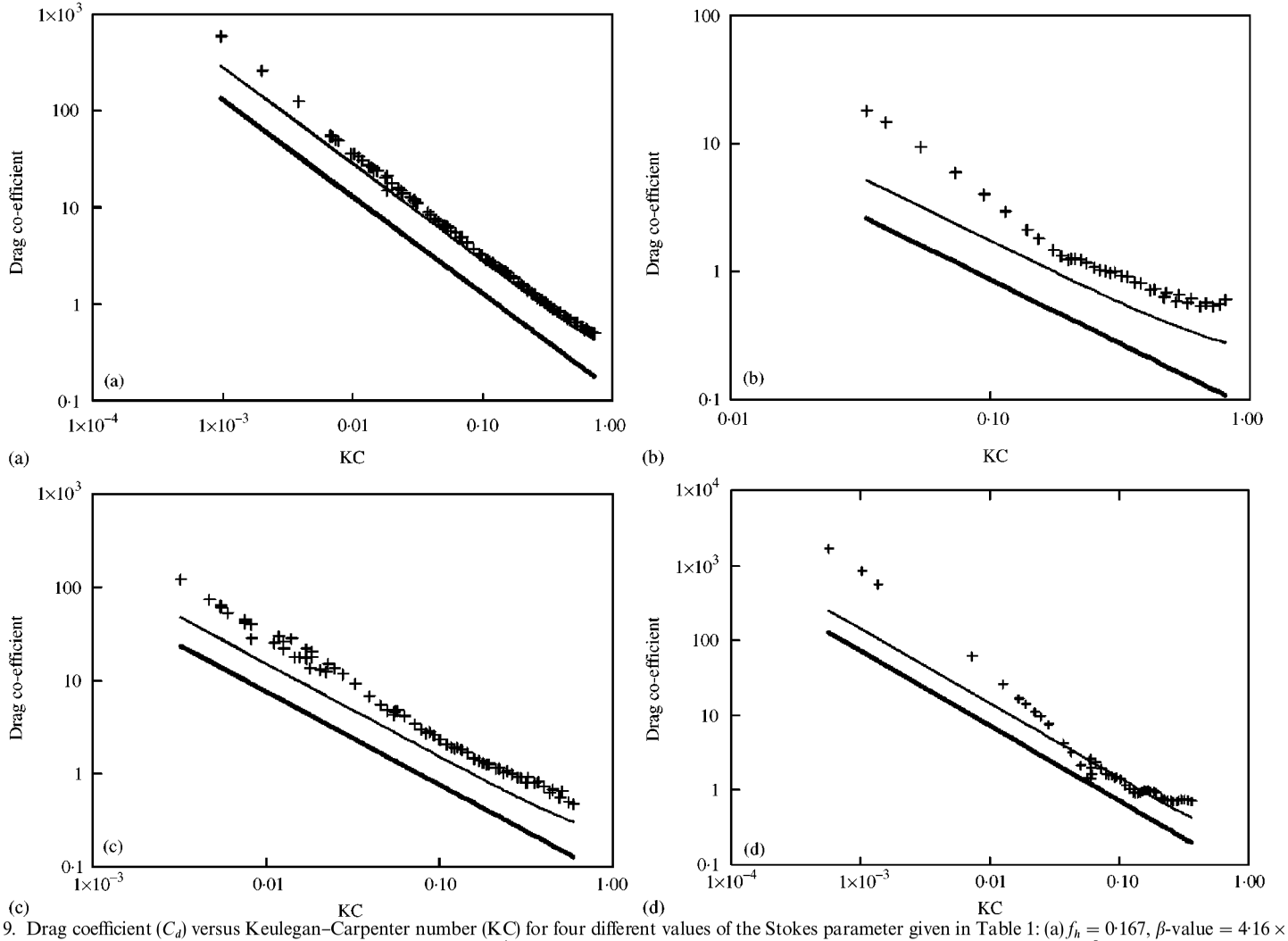

Figure 9. Drag coefficient (C_d) versus Keulegan–Carpenter number (KC) for four different values of the Stokes parameter given in Table 1: (a) $f_h = 0{\cdot}167$, β-value $= 4{\cdot}16 \times 10^4$, $\zeta_{r_h} = 0{\cdot}142$, $\zeta_{r_v} = 0{\cdot}136$ and $\zeta_{r_w} = 0{\cdot}006$; (b) $f_h = 0{\cdot}366$, β-value $= 9{\cdot}13 \times 10^4$, $\zeta_{r_h} = 0{\cdot}226$, $\zeta_{r_v} = 0{\cdot}123$ and $\zeta_{r_w} = 0{\cdot}103$; (c) $f_h = 0{\cdot}470$, β-value $= 1{\cdot}17 \times 10^5$, $\zeta_{r_h} = 0{\cdot}290$, $\zeta_{r_v} = 0{\cdot}114$ and $\zeta_{r_w} = 0{\cdot}176$; (d) $f_h = 0{\cdot}548$, β-value $= 1{\cdot}37 \times 10^5$, $\zeta_{r_h} = 0{\cdot}334$, $\zeta_{r_v} = 0{\cdot}095$ and $\zeta_{r_w} = 0{\cdot}239$. + +, Experimental; ——, prediction (Wang); —, prediction (2W).

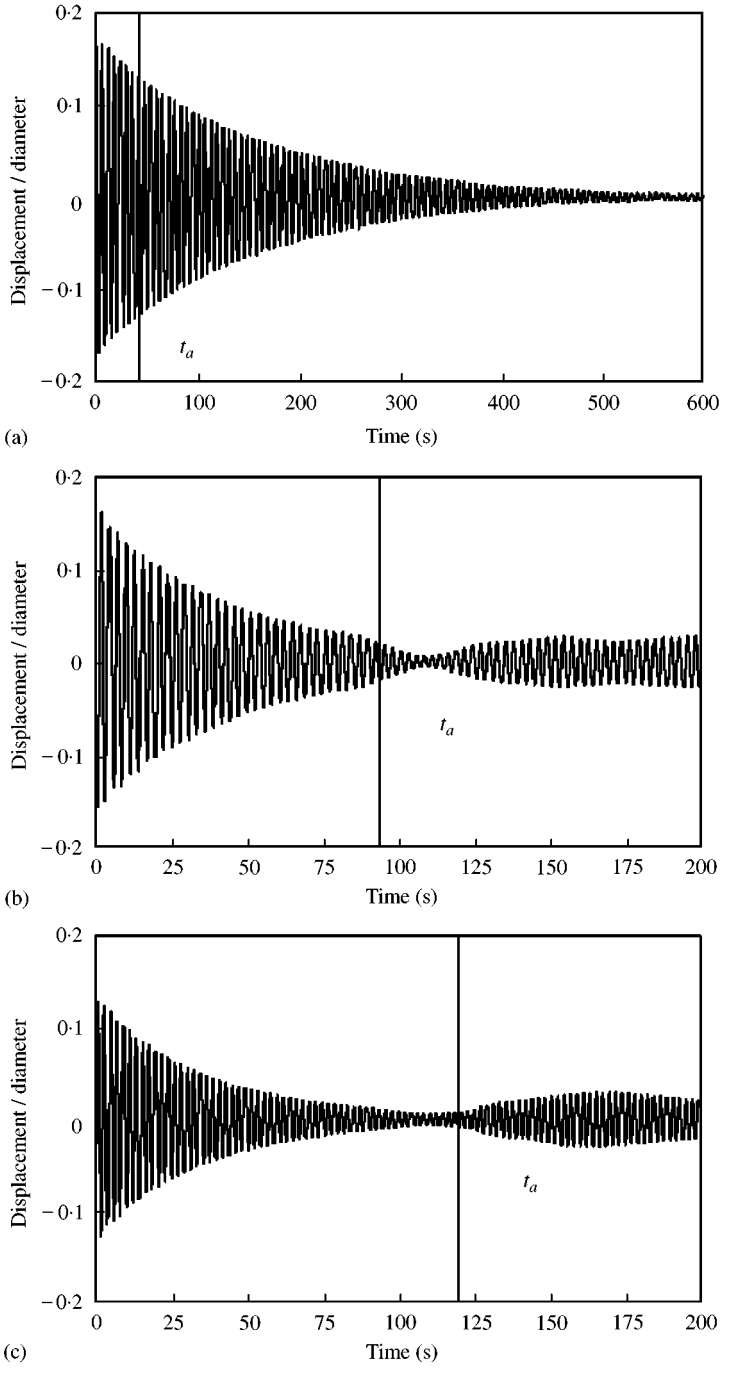

Figure 10. (a) Decaying oscillation for SP00 ($f = 0{\cdot}167$ Hz, $c = 9{\cdot}35$ m/s, $t_a = 43$ s). (b) Decaying oscillation for SP02 ($f = 0{\cdot}366$ Hz, $c = 4{\cdot}27$ m/s, $t_a = 94$ s). (c) Decaying oscillation for SP04 ($f = 0{\cdot}470$ Hz, $c = 3{\cdot}32$ m/s, $t_a = 120$ s).

and the surface finish of the cylinder. There will be a separation of flow at the end of the cylinder leading to increased hydrodynamic damping. Overestimates of the drag coefficients will arise if the structural damping is underestimated and possible reasons have been

discussed earlier. The least smooth variation of C_d with KC is noted for the highest frequency value plotted in Figure 9d. This is thought to be due to the influence of the higher structural mode at 2 Hz.

A further problem that was encountered was the effect on the cylinder motion of waves reflected from either end of the tank. The range of the KC-number over which measurements were made had to be limited for experiments carried out at $f = 0{\cdot}366$, $0{\cdot}470$ and $0{\cdot}548$ Hz as the amplitude of the cylinder motion was observed to increase at a certain time after the cylinder was released. This is quite clear from the traces presented in Figure 10(b,c). This increase in amplitude is due to the waves excited by the motion of the cylinder travelling to the ends of the tank and being reflected back to the cylinder. A concrete beach at one end of the tank and a wave paddle at the other were unable to completely absorb the radiated waves.

The wave celerity was calculated using linear wave theory and, with the knowledge that the distance to either end of the tank was 100 m, the time taken for the first radiated wave to return to the cylinder was estimated. The vertical line in each plot of the amplitude of the cylinder in Figure 10(a–c) gives the calculated time for the first wave crest to return. It can be seen in Figure 10(b,c) that there is a change in the amplitude behaviour at this time. However, in Figure 10(a), for the lowest oscillation frequency, no change is apparent. This is consistent with the results plotted in Figures 5 and 8 which show minimal radiation damping, and hence radiated waves, for the lowest frequency value. The precise behaviour of the suspended cylinder to returning waves will depend on their phase relative to the cylinder motion. For example, in Figure 10(b) the damping is observed to increase when the first waves return and then the cylinder is excited.

The hydrodynamic damping for a surface-piercing cylinder is shown to be a combination of viscous damping and radiation damping. Hence, if we wish to predict the damping of a full scale structure, the two components of damping need to be calculated separately, for the relevant conditions, and then combined. Returning to the example given at the beginning of the paper, a circular cylinder with a diameter of 10 m and a natural frequency of $0{\cdot}3$ Hz, then to use the results presented here the water depth is taken to be 100 m. This gives a value of a/h of $0{\cdot}05$ and therefore the results plotted in Figure 5 can be used directly. $\omega^2 a/g = ka = 1{\cdot}81$ and hence the radiation damping factor is $0{\cdot}0045$. The value of β appropriate to this cylinder is 3×10^7 and assuming that the empirical result in equation (4) applies and the mass ratio of the cylinder is the same as that used in the present experiments, then the viscous damping factor is $0{\cdot}00014$. Hence, compared to radiation damping, it is small enough to be neglected.

5. CONCLUSIONS

Experiments have been carried out on a $0{\cdot}5$ m diameter cylinder, piercing the water surface, to measure hydrodynamic damping. β values up to $1{\cdot}37 \times 10^5$ have been achieved and results are obtained for KC values as low as 10^{-3}. The total damping is a combination of structural, wave radiation and viscous damping. The structural damping has been measured and the radiation damping found from an analytical solution due to Dalrymple & Dean (1972). The viscous damping is estimated by subtracting these two components from the measured total damping. The viscous damping is also presented as a drag coefficient and the variation of this coefficient with KC is shown. The variations of the drag coefficient with β and KC are in general agreement with those measured on a fully submerged cylinder by Bearman & Russell (1996) and Chaplin & Subbiah (1996). In line with results from other authors, it is observed that the results for viscous damping are influenced by the surface finish of the cylinder.

ACKNOWLEDGEMENTS

This paper is dedicated to the late David Maull and the subject of fluid loading of offshore structures is one of many to which he made a significant contribution. Two of the authors, (PWB and JMRG), wish to record the influence of David in stimulating their interest in fluid dynamics through his insight and his deep understanding of the subject.

This work forms a part of the research programme carried out in the Delta Flume at Delft Hydraulics sponsored by the EC 'TMR Access to Large-Scale Facilities' Programme. The design and construction of the apparatus and the support of one of the authors, (LJ), was funded by the EPRSC. The authors express their thanks to the staff at Delft Hydraulics for their help during the test period and to J.P. Meggyesi who was in charge of constructing the pendulum rig.

REFERENCES

BEARMAN, P. W. & RUSSELL, M. P. 1996 Measurements of hydrodynamic damping of bluff bodies with application to the prediction of viscous damping of TLP hulls. *21st Symposium On Naval Hydrodynamics*, Trondheim, Norway, pp. 61–73.

BEARMAN, P. W. & MACKWOOD, P. R. 1992 Measurements of the hydrodynamic Damping of Oscillating Cylinders. *Proceedings of the 6th International BOSS Conference*, pp. 405–414.

BEARMAN, P. W., DOWNIE, M. J., GRAHAM, J. M. R. & OBASAJU, E. D. 1985 Forces on cylinder in viscous oscillatory flow at low Keulegan–Carpenter numbers. *Journal of Fluid Mechanics* **154,** 337–356.

CHAPLIN, J. R. & SUBBIAH, K. 1996 Hydrodynamic damping in the presence of oscillatory and steady flows. Final report to the ULOS programme.

CHAPLIN, J. R. & SUBBIAH, K. 1998 Hydrodynamic damping of a cylinder in still water and in a transverse current. *Applied Ocean Research* **20,** 251–259.

CHAPLIN, J. R., RAINLEY, R. C. T. & YEMM, R. W. 1997 Ringing of a vertical cylinder in waves. *Journal of Fluid Mechanics* **350,** 119–147.

DALRYMPLE, R. A. & DEAN, R. G. 1972 The spiral wavemaker for littoral drift studies. *Proceedings 13th Coastal Engineering Conference* (*ASCE*), pp. 689–705.

DEAN, R. G. & DALRYMPLE, R. A. 1993 Water wave mechanics for engineers and scientists. Vol. 2. Singapore, London: World Scientific, pp. 170–185.

HONJI, H. 1981 Streaked flow around an oscillating circular cylinder. *Journal of Fluid Mechanics* **107,** 509–520.

MEI, C. C. 1983 The applied dynamics of ocean surface waves. New York, Chichester: Wiley, pp. 300–304.

OTTER, A. 1990 Damping forces on a cylinder oscillating in a viscous fluid. *Applied Ocean Research* **12,** 153–155.

SARPKAYA, T. 1995 Hydrodynamic Damping, Flow-Induced Oscillations, and Biharmonic Response. *ASME Journal of Offshore Mechanics and Arctic Engineering* **117,** 232–238.

SARPKAYA, T. 1986(a) Force on a circular cylinder in viscous oscillatory flow at low Keulegan–Carpenter numbers. *Journal of Fluid Mechanics* **165,** 61–71.

SARPKAYA, T. 1986(b) In-line and transverse forces on smooth and rough cylinders in oscillatory flow at high Reynolds number. Tech. Report No. NPS-69-86-003, Naval Postgraduate School, Monterey, CA, U.S.A.

SARPKAYA, T. & ISAACSON, M. 1981 Mechanics of wave forces on offshore structures. New York: Van Nostrand Reinhold, pp. 435–445.

SARPKAYA, T. 2000, private communication.

STOKES, G. G. 1851 On the effect of the internal friction of fluids on the motion of pendulums. *Transactions of the Cambridge Philosophical Society* **9,** 8–106.

WANG, C. Y. 1968 On high frequency oscillating viscous flows. *Journal of Fluid Mechanics* **32,** 55–68.